34th Annual International Conference of the IEEE EMBS
San Diego, California USA, 28 August - 1 September, 2012

Subzone based multi-frequency magnetic resonance elastography using a Rayleigh damped material model

Andrii Petrov[1], Geoffrey Chase[1], Mathieu Sellier[1], Peter Latta[2],
Marco Gruwel[2], Matthew McGarry[3] and Elijah Van Houten[4]

***Abstract*— MR Elastography (MRE) is a relatively novel imaging technique using conventional MRI methods to assess the mechanical properties of tissues. In time-harmonic MRE, a Rayleigh, or *proportional*, Damping (RD) model incorporates attenuation behavior proportionally related to both elastic and inertial forces, thus providing a more sophisticated description of the elastic energy dissipation occurring in the biological tissue. The overall damping ratio can be extracted from the combined effect of these two components, while an additional measure, called *Rayleigh Composition*, can be calculated by the ratio between the two components. Thus, RD elastography is capable of not only reconstructing the viscoelastic properties of the material, but also providing additional information about damping behavior and structure.**

A 3D subzone based reconstruction algorithm using a RD material model has been developed and optimized to reconstruct the viscoelastic properties, damping behavior and elastic energy attenuation mechanism of tissue-simulating damping phantoms across multiple frequencies. Results have shown that all three iterative reconstructed parameters are in relatively close agreement for both the tofu and gelatin materials in both phantom configurations across the frequency range. Preliminary results from in-vivo healthy brain are also presented and discussed.

I. INTRODUCTION

Magnetic Resonance Elastography (MRE) is a non-invasive medical imaging modality able to quantify the distribution of soft tissue elasticity deduced from 3D displacement measurements within the tissue obtained by phase-contrast Magnetic Resonance Imaging (MRI) techniques. Applied to biological tissue, MRE is believed to have potential application in the detection and diagnosis of a wide variety of pathologies, diseases and cancer formations, especially tumors.

The majority of tissue damping models currently used in elastography are based on Hookean elasticity and linear viscoelasticity assumptions of mechanical material behavior where attenuation forces are proportional to the elastic forces, thus modeling only a single damping effect. A Rayleigh Damping (RD) model applied to MRE treats both shear modulus and density as complex valued, assuming attenuation forces proportional to both elastic and viscous forces in the material [1]. The RD material model allows two damping parameters to be extracted from an MRE motion dataset and provides a more complex description of the elastic energy attenuation occurring in the tissue under time-harmonic actuation. Since the true nature of damping present in the *in vivo* biological tissue occurs due to the complex, multiscale interactions between microstructural tissue elements, it incorporates aspects related to both elastic and inertial forces. Therefore, such an extended damping description is appropriate for MRE applied to soft biological tissues. Thus, RD based elastography can reconstruct both VE properties and valuable damping information through an optimization process to provide a more sophisticated material structure description.

This study evaluates the performance of the subzone based, multi-frequency MRE using a RD material model [2] to accurately reconstruct structural, damping and stiffness characteristics of tissue-simulating damping phantoms and *in-vivo* healthy brain.

II. MATERIALS AND METHODS

A. Tissue-simulating phantom studies

Three tissue-simulating phantoms (1 undamped and 2 heterogeneous damping phantoms) were manufactured to investigate the performance of the reconstruction algorithm.

The undamped phantom (ND1 onwards) was made of an agarose gel material and had a cylindrical shape with two spherical inclusions of a higher stiffness (0.75% agarose gel concentration) than the background material (0.5 % agarose gel concentration). The phantom was actuated by a probe-type acoustic actuator [3]. The experiment was conducted for a mechanical frequency of 100 Hz. The single shot, spin-echo (SE) EPI images were acquired with the following parameters: TR/TE = 3000/120ms; field of view (FOV) = 190×190 mm; resolution of 128×128 pixels; and 17 slices of 3 mm thickness. The motion was encoded with three sinusoidal-shaped motion encoding gradient (MEG) cycles of 32 mT/m magnitude in 8 equally spaced time increments. Each time increment was acquired twice each time, using opposite MEG amplitude to eliminate phase wrapping.

The first damping phantom (D1 onwards) was made of soft tofu background with a single, stiff gelatin inclusion (10% Sigma Aldrich). The second damping phantom (D2 onwards) was a reverse configuration of D1 made of a stiff 10% gelatin background and a soft tofu inclusion. Both phantoms had

[1] A Petrov, M Sellier and G Chase are with the Department of Mechanical Engineering, University of Canterbury, Christchurch, New Zealand andrew.petrov@pg.canterbury.ac.nz

[2]P Latta is with the Institute for Biodiagnostics, National Research Council of Canada, Winnipeg, Canada; Institute of Measurement Science, Slovak Academy of Sciences, Bratislava, Slovakia

[2]M Gruwel is with the Institute for Biodiagnostics, National Research Council of Canada, Winnipeg, Canada

[3]M McGarry is with the Thayer School of Engineering, Dartmouth College, Hanover, New Hampshire, USA

[4]E Van Houten is with the Department of Mechanical Engineering, Universit de Sherbrooke, Sherbrooke, Quebec, Canada

a rectangular outside shape with the cylindrical inclusion located at the centre. The damping phantom studies were performed on a 1.5T Philips MRI scanner. Acoustic actuation was utilized to introduce shear waves into the phantoms at multiple mechanical frequencies of 50 Hz, 75 Hz, 100 Hz and 125 Hz. 20 coronal slices of 3 mm thickness of 3D steady state displacement fields were acquired by a SE based phase-contrast sequence, extended with trigger timing and MEG modules, using the following parameters: TR/TE = 480/10 ms; FOV = $150 \times 225 \times 40$ mm and 2 mm isotropic voxel. A 3D quality-guided phase unwrapping method [4] was applied to the motion MRE data to suppress phase wrapping.

Dynamic mechanical analysis (DMA), using a TA instruments Q800 Device with measurements at 100 Hz, was performed to provide a quantitative comparison between elastic property measurements for gelatin and tofu phantom materials (Table 1).

B. In-vivo brain studies

In vivo brain experiments were performed on a 3T Tim Trio Siemens MRI scanner using a standard single channel head coil. Vibrations were induced via two pressure actuated drivers (PADs), placed under the subject's head in the MRI head coil. Two active subwoofers, modified with airtight acrylic lids, were used to generate acoustic waves delivered through long tubing to the PADs [3]. 10 slices of the 3D displacement fields were acquired by a single shot SE EPI sequence, extended with sinusoidal-shaped MEG modules of 32 mT/m magnitude, using the following parameters: TR/TE = 3000/120ms; FOV = 220×220 mm; resolution of 128×128 pixels. Isochromatic displacements were encoded with one MEG cycle in 8 equally spaced time increments.

The octahedral shear strain (OSS) signal to noise (SNR) [5] was obtained for phantom and brain data sets. Reconstruction computations were carried out on parallel supercomputing environment Blue Fern P575. A 3D subzone based reconstruction algorithm using an RD material model [2] was applied to reconstruct complex shear stiffness, a Rayleigh Composition (RC), ξ_{CSM}, and damping ratio (DR), ξ_d.

III. RESULTS AND DISCUSSION

A. Phantom studies

Fig. 1 shows results from the subzone based reconstruction algorithm of the first slice of ND1. Fig. 1(a) shows a T2-weighted MR magnitude image. Fig. 1 (b) and (c) illustrates the real and imaginary shear modulus image, μ_r and μ_i, respectively. The algorithm accurately mapped the presence and geometry of stiffer inclusions. Considering the physical dimensions of the inclusions it is evident that the algorithm is able to reconstruct small-scale areas with low stiffness contrast. Reconstructed values fall within expected ranges. Fig. 1 (d) depicts the damping ratio, ξ_d, indicating attenuation within the phantom. The inclusions are clearly depicted by two areas with low damping, indicating low energy loss confirming the presence of stiffer materials. Fig. 1 (c) shows the RC, ξ_{CSM}, image which represents a relative measure of the damping mechanism. The phantom was constructed entirely of gelatin and thus the lack of strong contrast in the ξ_{CSM} image is in agreement with expected physical behavior of gelatin.

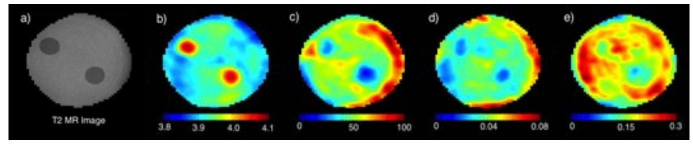

Fig. 1. RD MRE reconstruction results performed on ND1 phantom using mechanical excitation at 100 Hz: (a) MR T2-weighted image; (b) μ_r image (kPa) ; (c) μ_i image (Pa) ; (c) ξ_d image (%100) and (d) ξ_{CSM} image (%100)

Fig. 2 shows T2-weighted MR images of D1 and D2 phantoms for reference. Inclusions can clearly be distinguished in both phantoms.

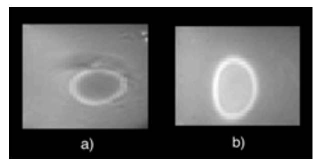

Fig. 2. T2-weighted MR image: (a) D1 phantom, consisting of a soft tofu background and a stiff gelatin inclusion (b) D2 phantom, consisting of a stiff gelatin background and a soft tofu inclusion

TABLE I

COMPARISON BETWEEN DMA AND MRE RESULTS FOR 10% GELATIN AND SOFT TOFU MATERIALS AT 100HZ

Material	Gelatin		Tofu	
Parameter	MRE	DMA	MRE	DMA
μ_R *(Pa)*				
P1	7087 ± 507	8800 ± 900	4678 ± 480	6368 ± 390
P2	7056 ± 757		5848 ± 421	
μ_I *(Pa)*				
P1	970 ± 606	294 ± 131	200 ± 204	
P2	318 ± 96		456 ± 187	

Fig. 3 and 4 demonstrate RD reconstruction results of the first slice (located near the actuator) from D1 and D2, respectively. To provide quantitative analysis between D1 and D2 reconstruction results, the inclusion and background were segmented to calculate the distribution of the property values. Table 2 shows the mean and standard deviation (SD) of each property within the selected region of interest (ROI). Acceptable correlation is evident between property values for gelatin and tofu materials in both phantoms across multiple frequencies.

Fig. 3 (a) shows the real part of the displacement field in the X direction. Higher frequencies enable shorter wavelength and therefore finer resolution of the reconstructed parameters. Fig. 3 and 4 (b) and (c) illustrates the real and imaginary shear modulus image, μ_r and μ_i, respectively. Qualitatively, μ_r reconstruction of both materials was successfull, correctly confirming higher stiffness of the gelatin inclusion than the background tofu material as expected. Opposite trends are observed in D2 where the tofu inclusion has a lower magnitude of the μ_r than the gelatin background

TABLE II

ROI ANALYSIS OF THE TOFU AND GELATIN MATERIALS IN D1 & D2 PHANTOMS ACROSS MULTI FREQUENCY DOMAIN

Frequency	50 Hz		75 Hz		100 Hz		125 Hz	
Parameter	D1	D2	D1	D2	D1	D2	D1	D2
μ_R (Pa)								
Tofu	4006 $\pm$ 145	4850 $\pm$ 225	4234 $\pm$ 236	5048 $\pm$ 285	4678 $\pm$ 480	5847$\pm$ 421	5332 $\pm$ 634	6110 $\pm$ 531
Gelatin	4309 $\pm$ 92	5095 $\pm$ 272	4815 $\pm$ 116	5817 $\pm$ 292	7087 $\pm$ 507	7056 $\pm$ 757	8561 $\pm$ 500	8696 $\pm$ 670
μ_I (Pa)								
Tofu	56 $\pm$ 67	57 $\pm$ 33	121 $\pm$ 102	189 $\pm$ 119	200 $\pm$ 204	456 $\pm$ 187	223 $\pm$ 241	202 $\pm$ 215
Gelatin	209 $\pm$ 127	64 $\pm$ 29	270 $\pm$ 73	238 $\pm$ 132	970 $\pm$ 606	318 $\pm$ 96	1107 $\pm$ 677	741 $\pm$ 325
ρ_I (kg/m^2)								
Tofu	-117 $\pm$ 115	-80 $\pm$ 28	-157 $\pm$ 93	-93 $\pm$ 89	-154 $\pm$ 208	-87 $\pm$ 126	-510 $\pm$ 471	-336 $\pm$ 405
Gelatin	-20 $\pm$ 24	-31 $\pm$ 9	-30 $\pm$ 10	-38 $\pm$ 15	-25 $\pm$ 54	-29 $\pm$ 20	-39 $\pm$ 85	-36 $\pm$ 54
ξ_d (%100)								
Tofu	0.066 $\pm$ 0.05	0.045 $\pm$ 0.015	0.09 $\pm$ 0.05	0.07 $\pm$ 0.04	0.1 $\pm$ 0.1	0.09 $\pm$ 0.06	0.27 $\pm$ 0.22	0.22 $\pm$ 0.28
Gelatin	0.034 $\pm$ 0.02	0.022 $\pm$ 0.006	0.04 $\pm$ 0.01	0.04 $\pm$ 0.013	0.08 $\pm$ 0.044	0.037 $\pm$ 0.01	0.083 $\pm$ 0.049	0.063 $\pm$ 0.03
ξ_{CSM}(%100)								
Tofu	0.20 $\pm$ 0.23	0.13 $\pm$ 0.06	0.18 $\pm$ 0.11	0.36 $\pm$ 0.27	0.36 $\pm$ 0.3	0.6 $\pm$ 0.23	0.18 $\pm$ 0.24	0.15 $\pm$ 0.2
Gelatin	0.72 $\pm$ 0.18	0.28 $\pm$ 0.10	0.65 $\pm$ 0.07	0.5 $\pm$ 0.17	0.85 $\pm$ 0.21	0.63 $\pm$ 0.15	0.79 $\pm$ 0.25	0.77 $\pm$ 0.23

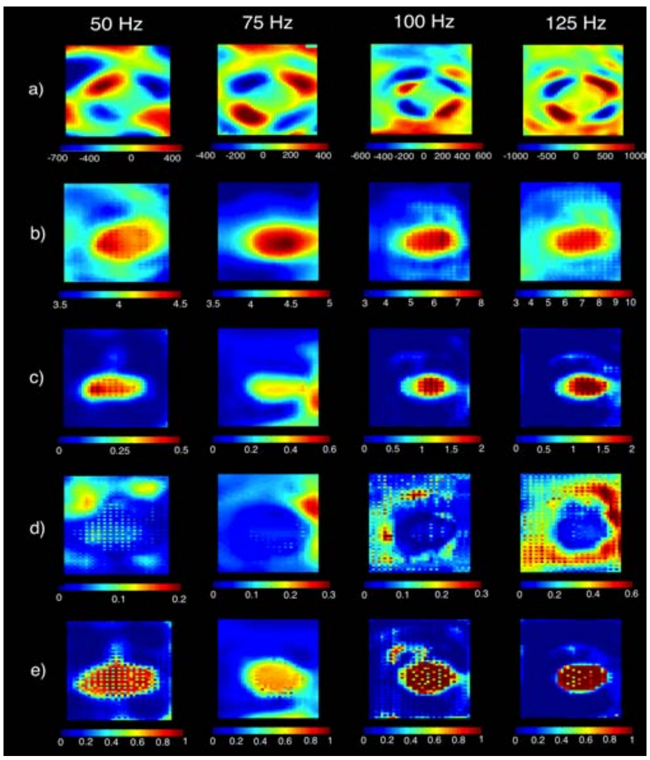

Fig. 3. RD MRE reconstruction results performed on D1 phantom configuration (soft tofu background, stiff gelatin inclusion) using multi frequency mechanical excitation: (a) real part of the displacement in the X direction; (b) μ_r image (kPa); (c) μ_i image (kPa); (d) ξ_d image (%100), indicating a relative measure of the attenuation; (e) ξ_{CSM} image (%100), representing a relative measure of the damping mechanism.

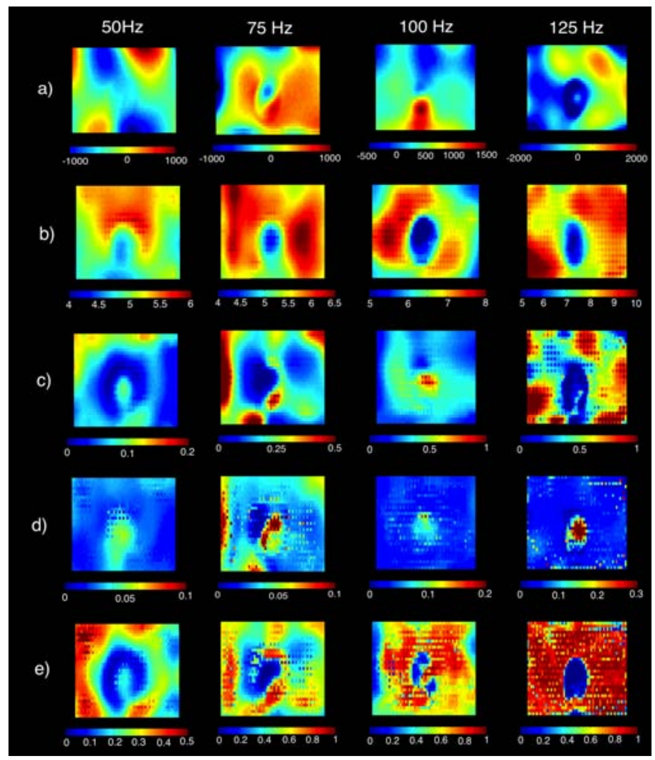

Fig. 4. RD MRE reconstruction results performed on D2 phantom configuration (stiff gelatin background, soft tofu inclusion) using multi frequency mechanical excitation: (a) real part of the displacement in the X direction; (b) μ_r image (kPa); (c) μ_i image (kPa); (d) ξ_d image (%100), indicating a relative measure of the attenuation; (e) ξ_{CSM} image (%100), representing a relative measure of the damping mechanism.

(Fig. 4(b)). In D1, reconstructions of the tofu background show a relative smooth distribution of the μ_r values, where the presence of the gelatin inclusion is clearly distinguishable (Fig. 3(b)). The μ_r distribution in D2 show some variation in the gelatin background stiffness values, while the tofu inclusion is easily located based on visual inspection of image (Fig. 4(b)). Also, μ_r values of the tofu and gelatin materials consistently increase in both phantoms with increasing frequency, which correlates well with the power law phenomenon. The variation in μ_r within the tofu material in both phantoms across multiple frequencies is relatively high (Table 2) and is greater than one standard deviation. In the case of the gelatin, discrepancy in the μ_r values is more prominent in the lower frequency range and almost negligible at the higher frequencies.

Fig. 3 and 4 (d) shows the reconstructed DR, ξ_d, image. The location of the inclusion is evident in the reconstructed ξ_d images in the both phantoms, although variations are present around the region of the inclusion and supposedly constant background area. Qualitatively, the ξ_d was reconstructed correctly for both materials over all frequencies. In D2 the magnitude of the ξ_d is increasing in the vicinity of tofu inclusion, correctly confirming higher loss of mechanical energy in the more attenuating tofu material compared to the stiffer gelatin background (Fig. 4(d)). In contrast, the gelatin inclusion in D1 has lower damping than the tofu background (Fig. 3(d)). Quantitative ROI analysis of the ξ_d shows good agreement for both materials across multiple frequencies in both phantoms (Table 2).

Fig. 3 and 4 (e) illustrates the reconstructed RC, ξ_{CSM}. Qualitatively, the location of the gelatin inclusion can be clearly distinguished within the tofu background in the reconstructed D1 RC image across the entire multi frequency range (Fig. 3(e)). Quantitative ROI analysis, given in Table 2, confirms noticeably different RD structure of the tofu background material compared to the gelatin inclusion material, with the gelatin inclusion having noticeably higher ξ_{CSM} values. In D2, ξ_{CSM} reconstruction had less success. For lower frequencies (50Hz, 75 Hz and 100 Hz) ξ_{CSM} seems to have significant variations in the vicinity of the tofu inclusion and in the area of the gelatin background, although the presence of the inclusion can still be distinguished (Fig. 4(e)). However, at the frequency of 125 Hz the ξ_{CSM} image is of very good quality. The presence of the tofu inclusion is clearly depicted in the low ξ_{CSM} values, while the stiffer gelatin background is reconstructed in the high ξ_{CSM} values. Some speckle noise is present, which is acceptable due to the nature of the MRE image acquisition. The results observed in both phantom configurations indicate that the high ξ_{CSM} values correspond to the tightly grouped, randomly arranged collagen strands of gelatin while low ξ_{CSM} values match fluid saturated structure of tofu. These results agree well with the previously reported by Van Houten *et al.* [2] studies of RD based elastography.

B. In-vivo brain results

Fig. 5 shows reconstruction results from a healthy *in vivo* brain computed by an isotropic, viscoelastic RD based material model. The anatomical structure of the ventricles can be distinguished in the μ_r image (Fig. 5(b)). Tab. 3 shows mean and SD of each property value of the segmented ventricles and intracranial matter. ROI analysis revealed that the central region of the brain about the ventricles exhibits much lower elasticity (~1kPa) than the surrounding white and gray regions (~2kPa) which is in agreement with expected near-zero shear modulus in the cerebrospinal fluid (CSF). The ventricles are clearly visible in Fig. 5 (f) as well, correctly indicating high loss of mechanical energy within the viscous CSF. Fig. 5 (g) also show change in ξ_{CSM} across different brain tissue types possibly providing a mechanism for differentiating tissue structure in addition to measuring elastic stiffness and attenuation. At this stage, it is too early to conclude whether ξ_{CSM} is able to differentiate between white and gray matter, suggesting further multifrequency elastography studies.

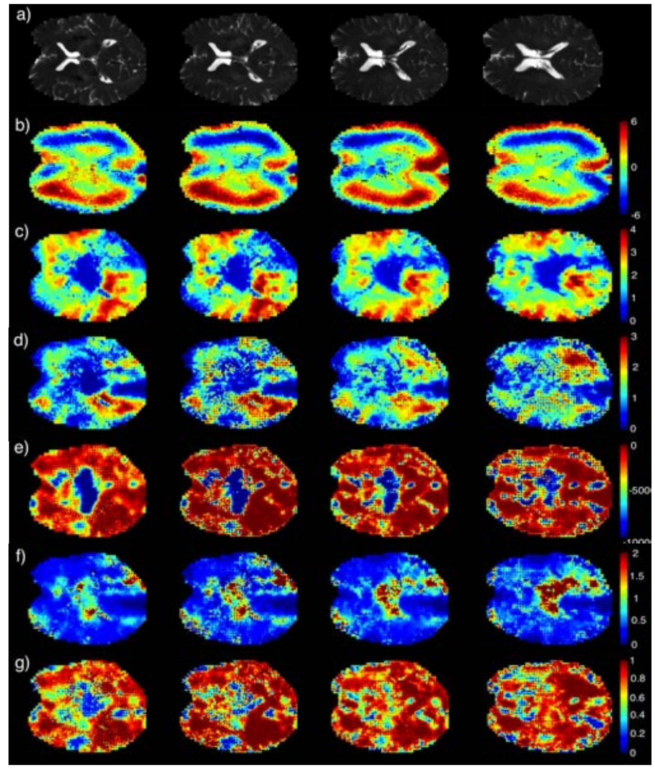

Fig. 5. RD MRE reconstruction results performed on a healthy human brain using 50 Hz mechanical excitation: (a) T2-weighted MR image for anatomical reference; (b) real part of the displacement image; (c) μ_r image (kPa), representing storage modulus; (d) μ_i image (kPa), representing loss modulus; (e) imaginary density, ρ_i, image (kg/m^2), which for incompressible case represents fluid flow out of the elastic matrix; (f) ξ_d image, indicating a relative measure of the attenuation in the brain tissue; (g) ξ_{CSM} image, representing a relative measure of the damping mechanism in the brain

TABLE III

ROI ANALYSIS OF THE IN-VIVO HEALTHY BRAIN

RD	μ_r (Pa)	μ_i (Pa)	ρ_i (kg/m^2)	ξ_d (%100)	ξ_{CSM} (%100)
Ventricles	1070 ± 778	1095 ± 738	-500 ± 427	1.07 ± 0.83	0.7 ± 0.25
White / Gray Matter	1992 ± 804	1150 ± 707	-281 ± 378	0.52 ± 0.48	0.72 ± 0.25

REFERENCES

[1] M. McGarry and E. Van Houten, "Use of a rayleigh damping model in elastography," *Medical and Biological Engineering and Computing*, vol. 46, no. 8, pp. 759–766, 2008.

[2] E. Van Houten, M. McGarry, P. Perrinez, I. Perreard, J. Weaver, and K. Paulsen, "Subzone based magnetic resonance elastography using a rayleigh damped material model," *Medical Physics*, vol. 38, pp. 1993–2004, 2011.

[3] P. Latta, M. Gruwel, P. Debergue, B. Matwiy, U. Sboto-Frankenstein, and B. Tomanek, "Convertible pneumatic actuator for magnetic resonance elastography of the brain," *Magnetic Resonance Imaging*, 2010.

[4] H. Wang, J. Weaver, I. Perreard, M. Doyley, and K. Paulsen, "A three-dimensional quality-guided phase unwrapping method for mr elastography," *Physics in Medicine and Biology*, vol. 56, pp. 3935–3942, 2011.

[5] M. McGarry, E. Van Houten, P. Perrinez, A. Pattison, J. Weaver, and K. Paulsen, "An octahedral shear strain-based measure of snr for 3d mr elastography," *Physics in Medicine and Biology*, vol. 56, pp. N153–N164, 2011.